

Updated Segmentation Model of the Aceh Segment of the Great Sumatran Fault System in Northern Sumatra, Indonesia

Aulia Kurnia Hady and Gayatri Indah Marliyani*

Department of Geological Engineering, Faculty of Engineering, Universitas Gadjah Mada, Yogyakarta, Indonesia

ABSTRACT. We study the Aceh Fault segment, the northernmost segment of the Great Sumatran Fault in western Indonesia. The Aceh Fault segment spans 250 km long, passing through three districts: West Aceh, Pidie Jaya, and Aceh Besar, a region of ~546,143 population. The current segmentation model assumes that the Aceh Fault segment acts as a single fault segment, which would generate closer to an M8 earthquake. This estimation is inconsistent with the ~M6–7 historical earthquake data. We conduct a detailed active fault mapping using an ~8 m resolution digital elevation model (DEM) of DEMNAS and sub-m DEM data from UAV-based photogrammetry to resolve this fault's segmentation model. Our study indicates that the Aceh Fault is active and that the fault segment can be further divided into seven sub-segments: Beutong, Kuala Tripa, Geumpang, Mane, Jantho, Indrapuri, and Pulo Aceh. The fault kinematics identified in the field is consistent with right-lateral faulting. Our study's findings provide new information to understand the fault geometry and estimate potential earthquakes' maximum magnitude along the Aceh Fault segment. These are important for the development of seismic hazard analysis of the area.

Keywords: Fault segmentation · Great Sumatran Fault · Earthquake hazards · Tectonic geomorphology · Aceh Fault.

1 INTRODUCTION

The seismically active right-lateral Great Sumatran Fault (GSF) is a major intra-continental transcurrent fault in western Indonesia. The fault accommodates most of the lateral motion of the 7 mm/year oblique convergence between the Indo-Australia and Eurasian plates at the Sunda subduction system (Curry, 2005; Singh *et al.*, 2013). The nearly 1650 km long, NW–SE oriented GSF stretches along the entire Sumatra Island from Semangko Bay at its NW point to Pulo Aceh Islands at its SE end. The fault consists of multiple segments, separated by geometric discontinuities (Sieh and Natawidjaja, 2000). The Aceh Fault segment is located at the northernmost part of the GSF. The north-

ern section of the GSF bifurcates into two fault systems: the Aceh and Seulimun faults ([Figure 1](#)). The junction between these two faults is associated with a transpressional structure indicated by elevated topography bounded by minor thrust faults. The Seulimun Fault stretches from Seulawah Agam volcano, continue on-shore to the Sabang Island ([Figure 1](#)). The Aceh Fault is separated from the Seulimun Fault by a ~4 km fault discontinuity (Tabei *et al.*, 2015). The Aceh Fault mainly traverses through three districts: West Aceh, Pidie Jaya, and Aceh Besar, and is located in close proximity of highly populated regions.

The Aceh Fault's current segmentation model indicates that the fault behaves as a single fault segment for its entire 250 km length, generating closer to an M8 earthquake (Sieh and Natawidjaja, 2000). This estimation is inconsistent with historical earthquake data, where most of the

*Corresponding author: G.I. MARLIYANI, Department of Geological Engineering, Universitas Gadjah Mada. Jl. Grafika 2 Yogyakarta, Indonesia. E-mail: gayatri.marliyani@ugm.ac.id

large earthquakes in the area are within ~M6-7 ranges. We reassess the segmentation model of the Aceh Fault by conducting detailed surface geomorphological and geological mapping of the fault (Figure 1).

For the active fault mapping, we implemented both remotely- and field-based mapping methods. We use an ~8 m resolution digital elevation model (DEM) from DEMNAS for our base map. This remotely-based mapping is then followed by field observations to confirm the fault trace and obtain the fault kinematic indicators. In addition, we also generate sub-meter resolution DEM using photogrammetry techniques of the aerial photos obtained using an unmanned aerial vehicle (UAV) at several sites. The purpose of this study is to refine the segmentation model and active fault map of the Aceh Fault to understand better the fault geometry and hazards associated with the fault.

2 GEOLOGY OF ACEH FAULT SEGMENT

The geology of the Aceh Fault zone has been documented by the Geological Survey Agency of Indonesia and is published in several 1:250,000 regional geology maps (Bennert *et al.*, 1981; Cameron *et al.*, 1983). The fault segment is covered by two map quadrangles: Banda Aceh (Bennert *et al.*, 1981) and the Taken-gon (Cameron *et al.*, 1983). The basement rock is mostly composed of Trias-Cretaceous age metamorphic rock and is well-exposed in the elevated regions (Figure 2). Sequences of deep-marine overlie the basement rock, covered by subsequent volcanic and turbiditic sediments. Recent volcanic products then cover all of these rock units. Krueng Aceh basin's lowland region is filled with young alluvium deposits composed of silt – gravel sediment (Moechtar *et al.*, 2009) (Figure 2). The strike-slip motion of the Aceh Fault creates several pull-apart basins in some areas along the fault. These basins are filled with Quaternary lake deposits, such as in Tangse and Geumpang area (Figure 2).

The Aceh Fault is indicated by a prominent straight and sinusoidal fault scarps in the topography. The fault is separated from Tripa Fault to the southeast by a 9 km wide restraining bend (Sieh and Natawidjaja, 2000) (Figure 1a). The northwestern section of the fault

passes through the low relief region of Banda Aceh; it continues offshore and merges with the Andaman Nicobar Fault (Curry *et al.*, 1979; Singh *et al.*, 2013). The offshore section of the Aceh Fault passes through the Pulo Aceh archipelago (Figures 1 and 3). The chain of the small islands of this archipelago is oriented parallel to the fault trend. Mapping by Fernandez *et al.* (2016) along this archipelago suggests that several E–W oriented reverse faults dominate the structural configuration of Pulo Aceh.

Sieh and Natawidjaja (2000) mapped the Sumatran Fault system based on the analysis of 1:50,000-scale topographic maps, 1:100,000-scale aerial photographs, and 1:250,000 geologic maps. Their study suggests that the Aceh fault segment is continuous.

3 METHODS

We conducted surface geology and geomorphology mapping using a ~8 m resolution DEM (and its derivative maps) from DEMNAS. The availability of the 8-m resolution DEM greatly increases our capabilities of recognizing active faults in the topography. Active faults can be recognized in the topography by the occurrence of young fault scarps, displacements of geomorphic features, and deformation of young sediments (Marliyani, 2016). To identify significant topographic breaks, we created a shaded-relief map of the area along the fault by combining four-light directions with a raster calculator tool in ArcGIS software. To trace the fault in the offshore area, we use a 185 m resolution bathymetry data from BATNAS. In areas where indications of surface faulting are prominent, we obtained aerial photographs using an unmanned aerial vehicle (UAV) and create high-resolution topography data using the structure from motion (SfM) procedure (Bemis *et al.*, 2014). The photomosaics obtained from the aerial survey were processed to generate a digital surface model (DSM). The DSM data are subsequently processed to generate digital terrain model (DTM) data using licensed Geomatica software. We use the data as a base map to analyze the area's tectonic geomorphology in greater detail.

We follow the mapping procedure described by Marliyani (2016). We begin our fault mapping by lineament analysis of the area. We de-

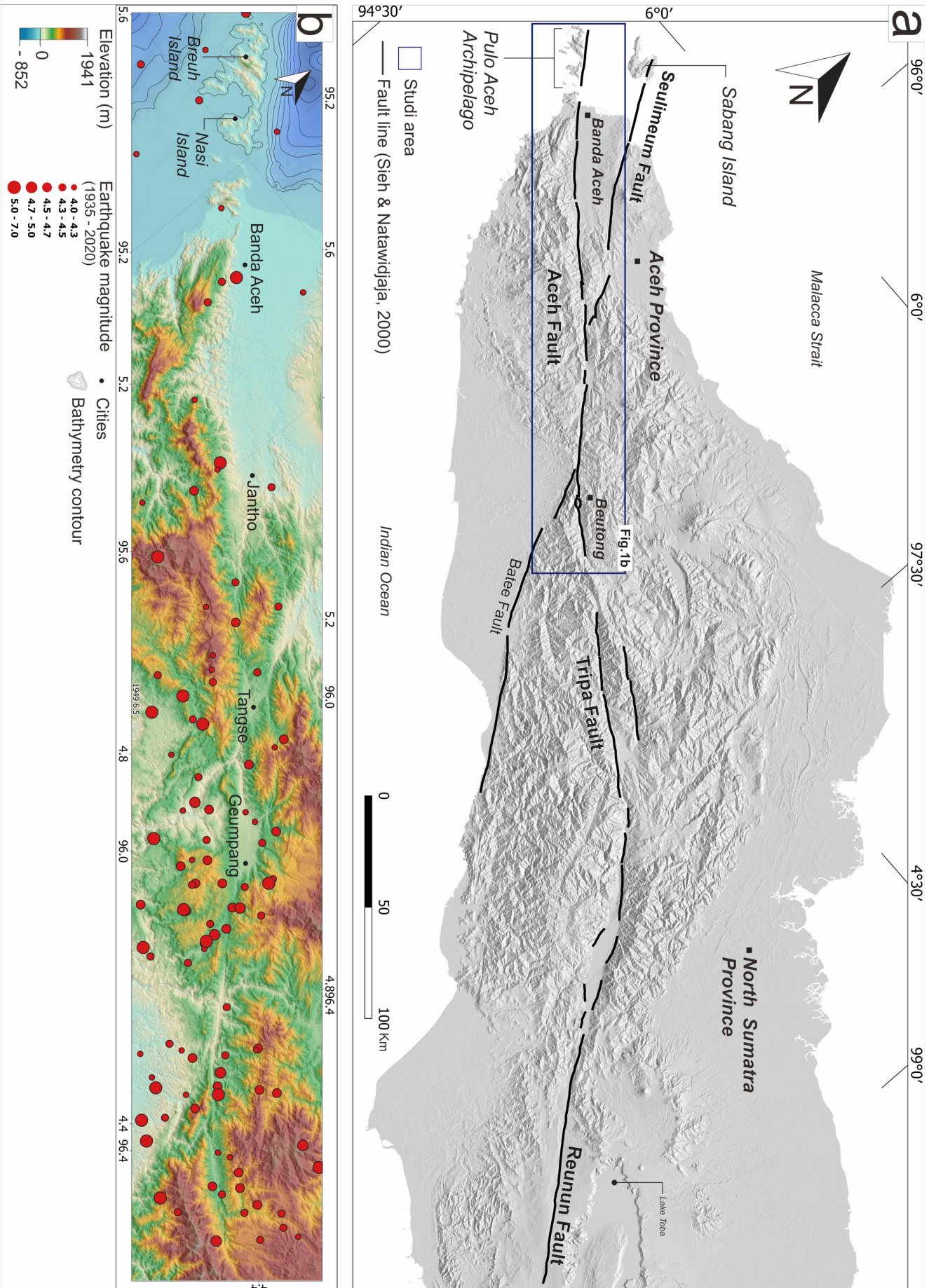


FIGURE 1. (a) Map of the Aceh Fault segment, blue polygon delineate our study area. (b) Map showing the epicenters of M4-6 shallow earthquakes along the Aceh Fault (red dots). Base maps are from the DEMNAS data. The earthquakes are from BMKG earthquake catalog.

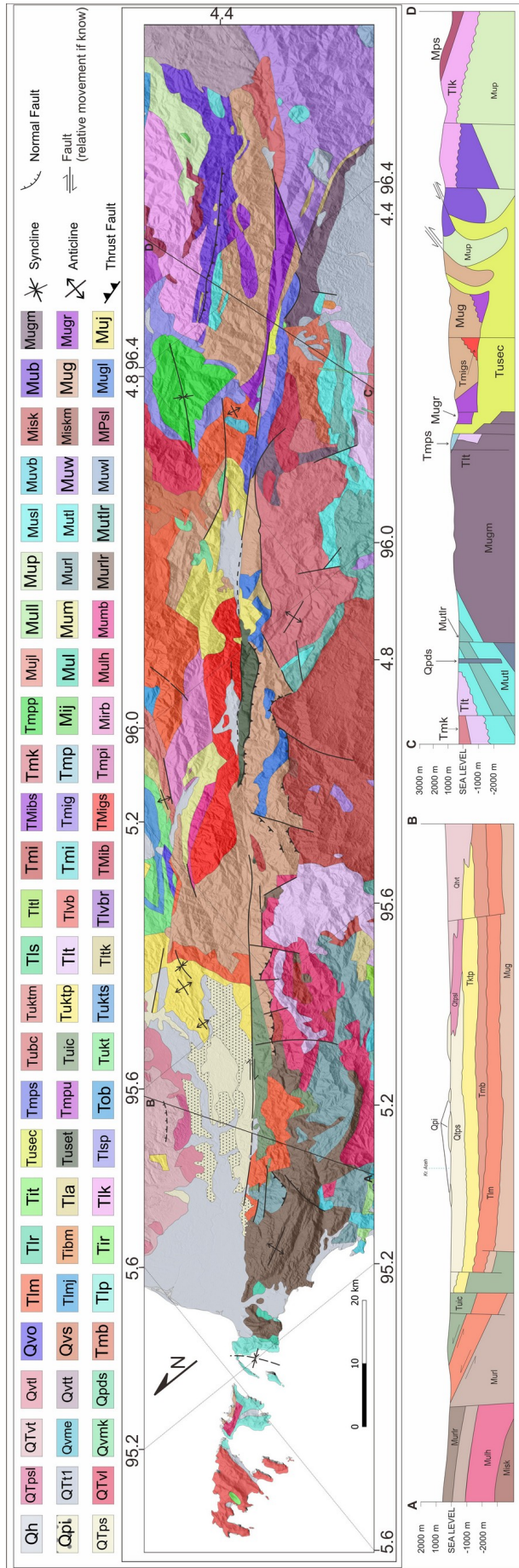


FIGURE 2. Simplified geological map of Aceh fault zone and their cross-sections (Bennett *et al.*, 1981; Cameron *et al.*, 1983). The lithology along the Aceh Fault zone mostly consists of Trias-Cretaceous metamorphic units. Quaternary deposits covered some of the lowland regions. Qh: young alluvium; Qp1: conglomerate of Idi Fm; Qp2: neritic sandstone of Seulimaum Fm; Qp3: reef limestone of Lam Kubue Member; Qp4: fluvial sandstone of Takengon Fm; Qp5: Qp6, Qp7, Qp8, Qp9, Qp10, Qp11, Qp12, Qp13, Qp14, Qp15, Qp16, Qp17, Qp18, Qp19, Qp20, Qp21, Qp22, Qp23, Qp24, Qp25, Qp26, Qp27, Qp28, Qp29, Qp30, Qp31, Qp32, Qp33, Qp34, Qp35, Qp36, Qp37, Qp38, Qp39, Qp40, Qp41, Qp42, Qp43, Qp44, Qp45, Qp46, Qp47, Qp48, Qp49, Qp50: Oligo and Peuet volcanic units of Peuet Sague, Temba, Meugeumiceng, Meukeub, Lam Teuba, Telago, Qpds: basalt, Qvo, Qvs: Oligo and Peuet volcanic units, Tmb: litoral mudstone of Baong Fm; Tmj and Tlm: fluvial sandstone of Meucampili formation; Tlp: litoral limestone of Peunasu Fm; Tlr: fluvial sandstone of Rampong Fm; Tibm: Bale Meuko granodiorite; Tir: Raya diorite; Tit: Tampeue intrusive rocks; Tla: inner sublittoral sandstone of Agam Fm; Tlk: Sublittoral sandstone and mudstone; Tusec and Tuset: serpentinite of Cahop and Tange complex; Tlsp: litoral mudstone of Sipopok Fm; Tmps and Tmpu: litoral siltstone of Peutu Fm; Tob: fluvial sandstone of Peutu Fm; Tubc and Tuic: deep marine melange of Beatang and Indrapuri complex; Tukt, Tuktp and Tuktm: various member of marine mudstone and siltstone of Kotabakti Fm; Tls: marine sedimentary units of Semelit Fm; Tlt, Tlti: fluvial sedimentary units of Tangla Fm; Tltk: Argillaceous limestone and calcareous sandstone of Keubang Fm; Tlvb, Tlvbr: Breueh and Brawan volcanics; Tmi, Tmib, Tmibs, Tmig: miscellaneous intrusions of Beurieung, Baso and Geunteu; Tmigs: diorites and microdiorites of Glaseuke complex; Tmk: marine sandstone and siltstone of Kueh Fm; Tmp, Tmpi, Tmpp: marine sandstone and siltstone Peutu; Tmij: Jamur Pisang gabbro; Mirb: Rob microgabbro; Mujl: slates and meta limestones of Jaleum Fm; Mul and Mulh: phyllite of Lhonga Fm; Mull: fossiliferous limestones of Lamno Fm; Mum and Mumb: limestone of Lam Minet Fm; Mup: deep marine metamorphic rocks of Penarum Fm; Muri: cherty limestone and shale of Raba Fm; Musl: carbonate of Sise Member; Mutl: carbonates of Teunom Fm; Muwb: Bentaro volcanics; Muw: metavolcanic rocks of Woyla Group; Muwl: undifferentiated limestone units; Misk: Sikuleh granite; Miskm: older batolith of Sikuleh complex; Mub: metasedimentary complex of Bale Fm; Mug: metamorphic rock units of Geumpang Fm; Mugl: limestone of Geumpang Fm; Mugm: metamorphic rock units of Gume Fm; Muj: slates and meta limestones of Jeuleum Fm.

lineate the lineaments based on the linear arrangements of morphological features such as rivers, valleys, and hills. Following the completion of the lineament mapping, we conduct field checking. We then combine our lineament map with results from field geological and geomorphological survey. During the fieldwork, we record kinematic data (the strike, dip, pitch, rake, and sense of relative motion of the fault) identified both in the bedrock and in the loose Quaternary sediments and analyzed their spatial distribution. The detailed map of active fault geometry will allow us to evaluate and update the fault segmentation model.

The fault segments are determined based on their discontinuity. The faults can be separated from one another by the occurrence of fault steps, bends, and/or abrupt changes in the fault's general strike. In general, two faults can be separated into different segments if the separation between the segments is wider than 4 km (Wesnousky, 2006; Duman and Emre, 2013; Marliyani *et al.*, 2013). This study uses the term "fault sub-segment" or "section" without implying any term particular to their geological or seismological significance. We use the term to indicate an updated model from the previously established segmentation model.

We estimate the maximum magnitude of the earthquake using an empirical model proposed by Stirling *et al.* (2008) to determine earthquake magnitude using fault surface length, as follow:

$$M_w = 4.18 + \frac{2}{3} \log W + \frac{4}{3} \log L \quad (1)$$

We are using the assumption of 16 km seismogenic depth and 80° of fault dip for our calculation. The seismogenic depth is estimated based on the maximum depth of recorded earthquakes along the fault, and the fault dip is based on the field observation.

4 RESULT

4.1 Lineament analysis

The Aceh Fault zone is represented in the topography as a series of linear ridges and valley, mostly in the NW–SE orientation with some minor N–S and E–W oriented lineaments (Figures 2 and 4). The lineaments are mostly recognized through the continuous break in elevation, which is likely to indicate fault scarps.

We also identified linear arrangements of offset channels, such as in Geumpang, Tangse, and Jantho (Figure 4). Their right separation of these channels is consistent with the Aceh Fault segment's orientation and sense of motion. Our lineament analysis shows that the Aceh Fault segment does not appear as a continuous fault throughout its 250 km length but rather separated into several 15–50 km length fault sections (Figure 3). Toward the northwestern end of the fault, near the Banda Aceh area, we identified smaller linear features, slightly deviate from the main NW–SE orientation fabrics (Figure 3).

In the following sections, we describe our lineament analysis along the fault. Our presentation's arrangement is based on the lateral distance from southeast to northwest, with the 0 km marked the southeast end of the fault and 250 km marked the northwest end (Figure 3).

Along km 0–13.8, the fault appears as a prominent narrow valley (Figure 3). There is no contrast topographic roughness and elevation on both sides of the fault (Figure 3). At km 12 to 16, the fault is visibly dissecting alluvial fan deposits. At km 25, a 2.5 km wide left step over formed a push-up ridge (Figure 3), this may act as a candidate for a fault segment boundary. At km 35, the fault scarp turns its orientation slightly to the north.

Starting at km 155, the fault formed a slightly sinusoidal shape (Figure 3). At km 155–178.8, the fault separates Quaternary alluvium from the ophiolitic basement rock. Based on our observation of the rock units from the regional geology map (Bennet *et al.*, 1981), the separation of the metamorphic rock cropping out on the opposing fault blocks in the Krueng Aceh basin yielded a distance of 27.3 km.

4.2 Field observations

We conduct field checking where we observe strong evidence in the topography of surface faulting and/or fault exposure to validate their occurrence, also in an area where the faults disturb Quaternary sediments. We performed detailed observation and mapping in a total of 26 sites along the fault. The locations of these sites are shown in Figures 3 and 5. We record in detail indications of fault kinematics (the orientation and types of the faults, fractures, and

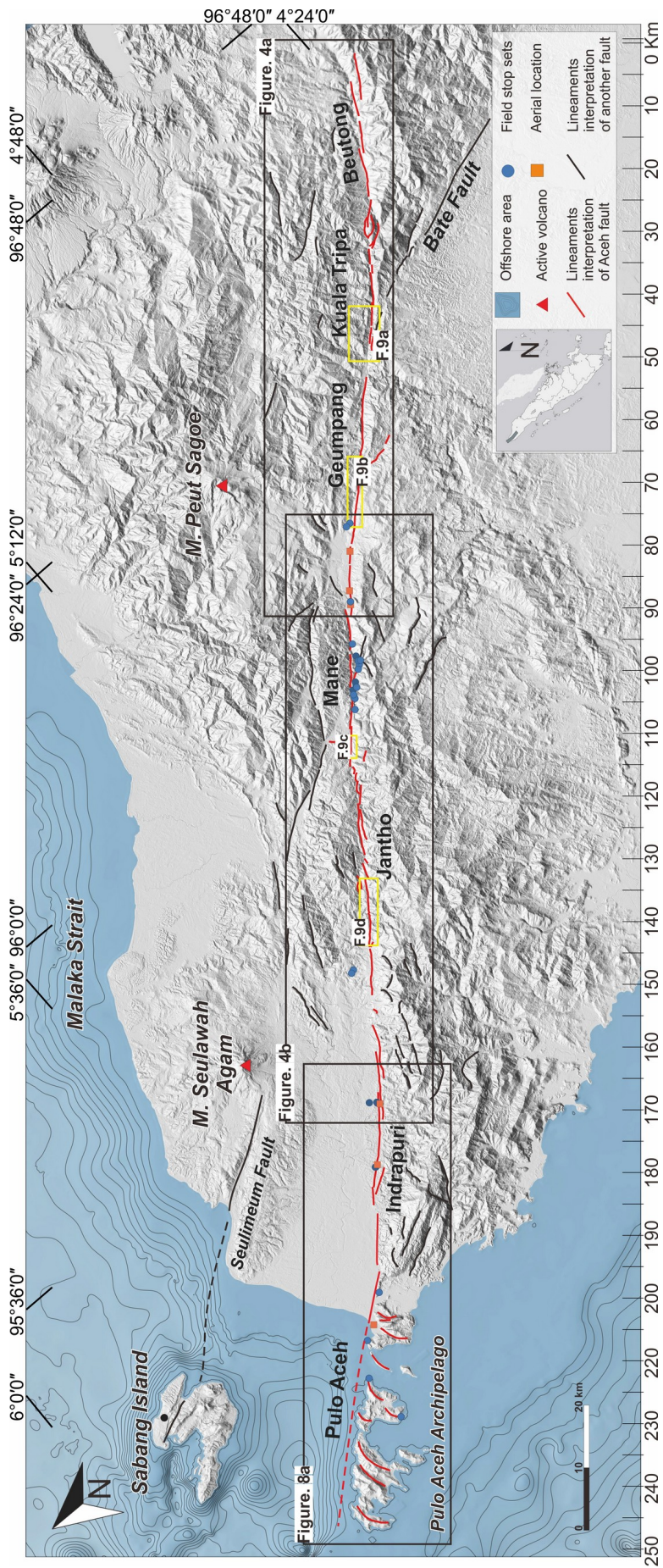


FIGURE 3. The lineament map along the Aceh Fault segment shows a dominant NW-SE trend. The shaded relief map is from DEMNAS. The bathymetry contour is adapted from BATNAS data.

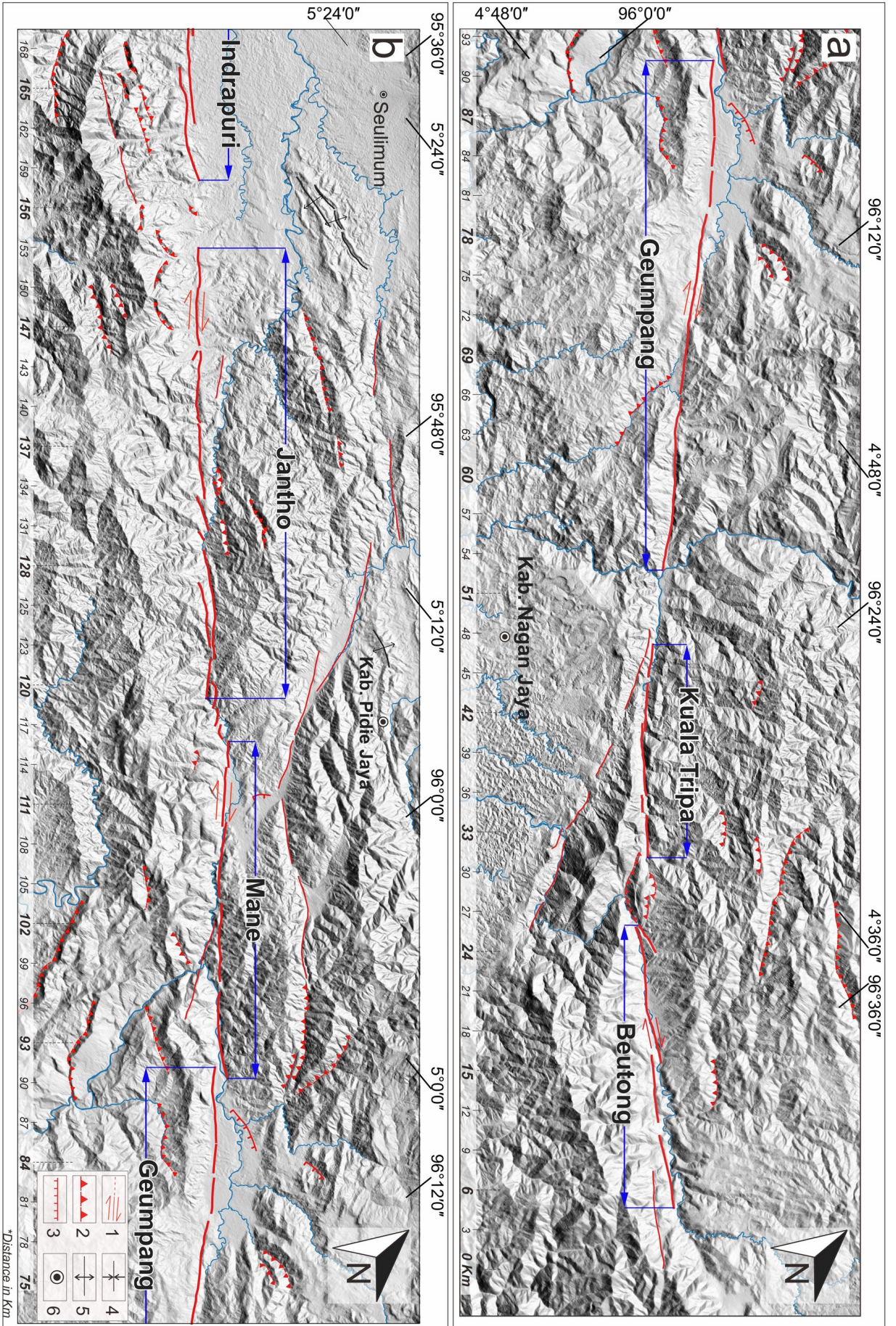


FIGURE 4. (a). Detailed map of the Beutong, Kuala Tripa, and Geumpang sub-segments. (b). Map of the Mane and Jantho sub-segment of the Aceh fault segment. Notation of the inserted legend: 1: right-lateral strike-slip fault; 2: reverse fault; 3: normal fault; 4: syncline; 5: anticline; 6: area/city.

folds) (Figures 5–8). In addition, we also collected aerial photos at several locations.

The nature of the strike-slip movement of the Aceh Fault creates a visible lateral offset in the topography. We identified several prominent features, such as channel offsets and shutter ridges. At some places, the systematic right-lateral offset of these features provides opportunities to calculate the cumulative offset and further calculate the fault (Figure 9).

Near Geumpang, at km 48–64.2, we observed narrow through with several left- and ~0.7 km-wide left- and right-step-overs. At km 77.5–90.9, we identify a fault that traversed an alluvial plain and forms a 3.3 km wide basin. At km 85.9, we identified a prominent offset channel and shutter ridge in the DEM data. We visited the area and confirmed that the channel was offset 12.7 m laterally. We took aerial photography using a drone to create a high-resolution topography data and recalculate the slip measurement using the newly developed DEM. The calculations are yielding multiple displacements ranging from 12.7 ± 2.1 to 48.4 ± 1 m (Figure 10).

At km 99.7 in the Mane area, a freshly opened roadcut exposing a fault zone dissecting a serpentinite metamorphic bedrock unit. At this location, the fault causing several landslides (Figure 6). About 250 m to the south, we observed indications of sinistral strike-slip faulting (Figure 6c). Between km 100.6–111, the fault runs through the alluvial plain. At km 106, we identified an offset channel. We calculated the separation using aerial photos, resolving a 108–127.8 m displacement. We identified several offset channels at km 126.2–138.3. The displacements are varied from 0.13–1.2 km. In these locations, the fault disturbed metamorphic rocks of Geumpang Formation.

At km 150–177, we identified a ~27 km channel offset. We identified a fault that disturbs the Quaternary volcanic rock unit at km 186 (Figure 8d). At km 174.5–175.2, we identified several prominent features, including a small-scale shutter ridge and wind gaps visible on the aerial photographs (Figure 8c).

At km 217.4, at Nasi Island, we observed an N 70° E trending fault plane. The fault is dipping to the NE and cutting through a layered sandstone unit of Peunasu Formation (Figure 6d). The fault is indicating reverse faulting

kinematics. In this area, we also observe evidence of recent deformation, where the fault appears to disturb Quaternary sediments (Figure 7a). We also identified several terrace deposits located ~20–40 m above the active channels (Figure 7b).

5 DISCUSSION

5.1 Sub-segmentation of Aceh Fault segment

Based on its geometrical configuration, we divided the Aceh Fault segment into seven sub-segments (from SE to NW): Beutong, Kuala Tripa, Geumpang, Mane, Jantho, Indrapuri, and Pulo Aceh (Figure 11). The separations of each fault segment are based on the occurrence of fault bends, steps, and changes in the direction of fault orientations. Nomenclature of the Aceh Fault segments' sub-segmentation follows geographical references of the region where the fault crosses, such as villages and rivers. We discuss each sub-segments in the following section, following their distance along the fault from its southeast end toward its northwest end.

The southeasternmost segment is the Beutong Fault. We identify the fault based on the occurrence of prominent linear topographic breaks. The fault is separated from the Tripa Fault to the southeast by a large restraining bend (~9 km). The 19-km long fault is oriented N306°E with several minor ~0.6–0.8 km wide step-overs along the fault. The geomorphological characteristics of the narrow valley (km 0–13.8), supported by field observations of several exposed fault planes, indicate right-lateral strike-slip fault kinematics.

The next fault segment to the northwest of Beutong Fault is the Kuala Tripa Fault. The total length of the Kuala Tripa Fault is 5.9–9.8 km. This sub-segment is separated from the Beutong Fault by a ~2.4 km wide restraining bend. At km 50, the fault meets another GSF segment called Bate Fault, generating a transpressional morphology (Figure 4a).

Continue to the northwest from Kuala Tripa, around km 50, is the Geumpang Fault sub-segment. The total length of this fault is 38.5 km. Although there are several step-overs identified along this fault, the step-overs are less than 1 km wide. Step-overs that are less than

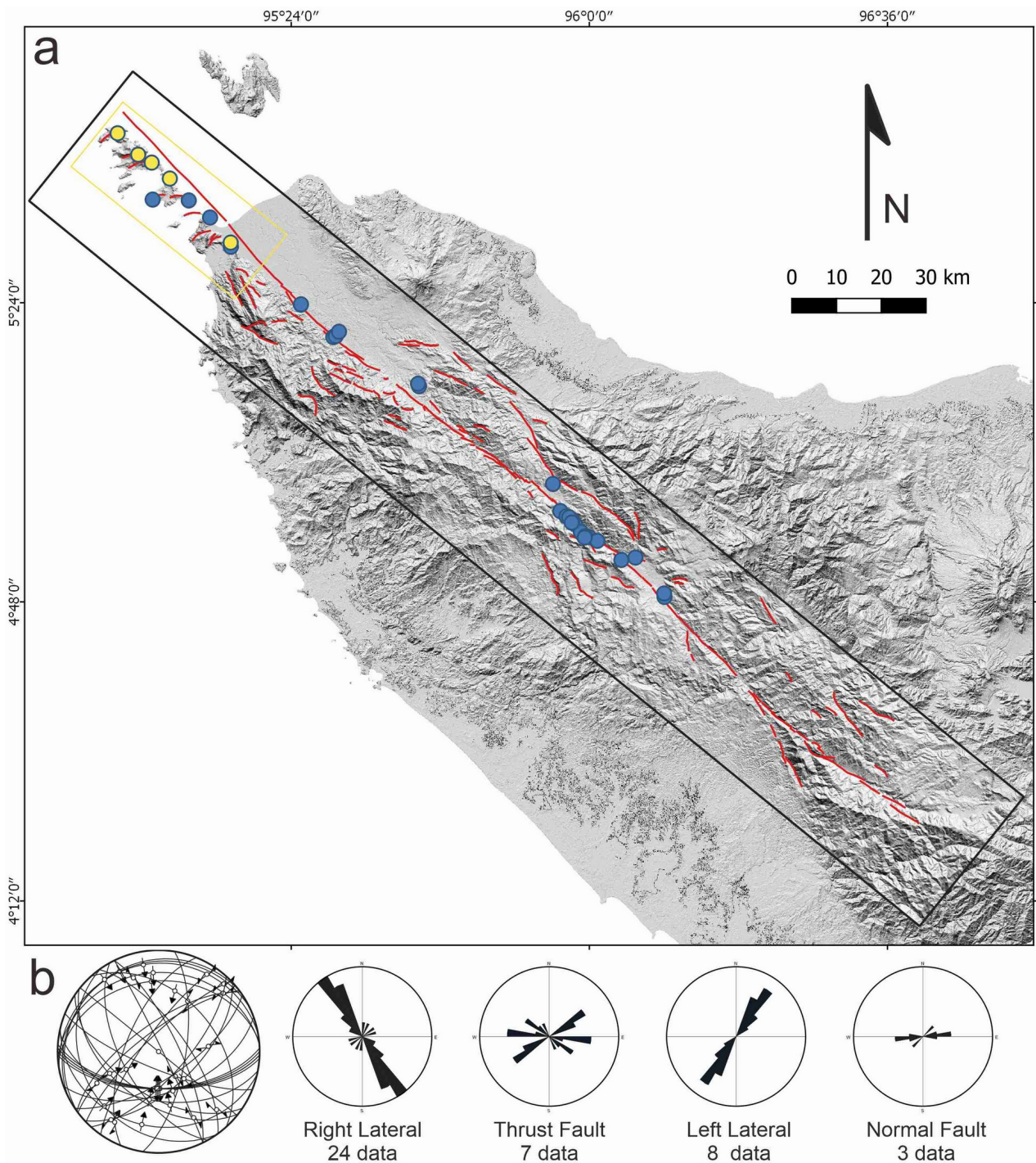


FIGURE 5. (a). Map showing the locations of field measurement of kinematic indicators (black polygon, blue dots). Yellow box delineates the study area of Fernández *et al.* (2016). Yellow dots mark measurement sites by Fernández *et al.* (2016). Red lines are lineaments identified during our remote and field-based mapping. (b) Schmidt lower hemisphere projection and rose diagram of the measured data.

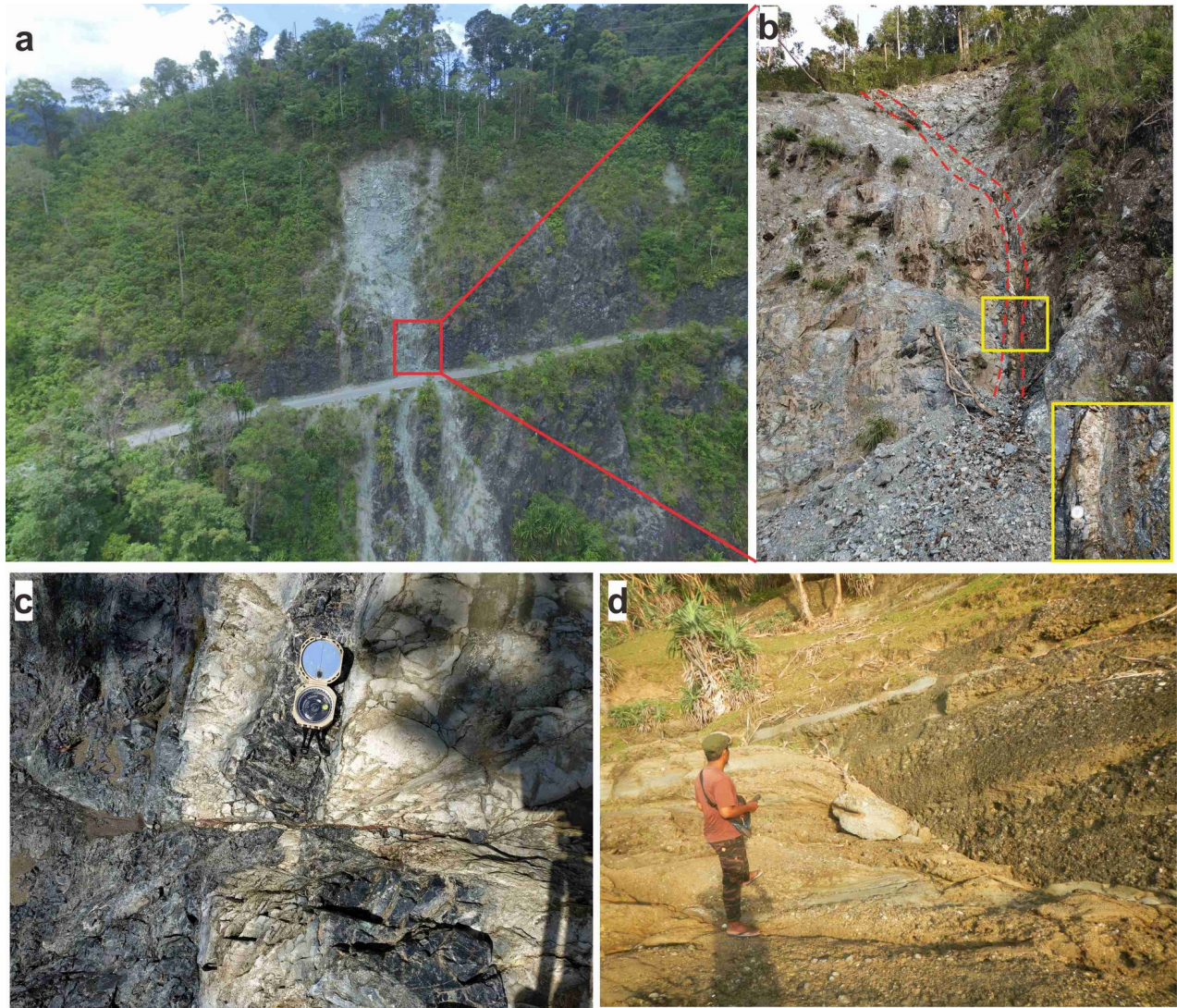


FIGURE 6. Documentation of faults exposed in bedrocks and deformed young alluvial terrace deposits along Aceh fault segment. (a) Fault trace associated with landslide zone along Mane sub-segments. (b) Outcrop photo of fault dissecting metamorphic bedrock exposed along a sub-district highway in the Mane area. The principal displacement zone (PDZ) is bounded by the red dashed line, the inserted photo (yellow border) display outcrops with a compass as a scale. (c) Exposure of a quartz vein cut by a left-lateral strike-slip fault at the upstream of the Woyla river in the Mane area. (d) Exposure of reverse fault showing an offset of stratigraphy in Nasi island.

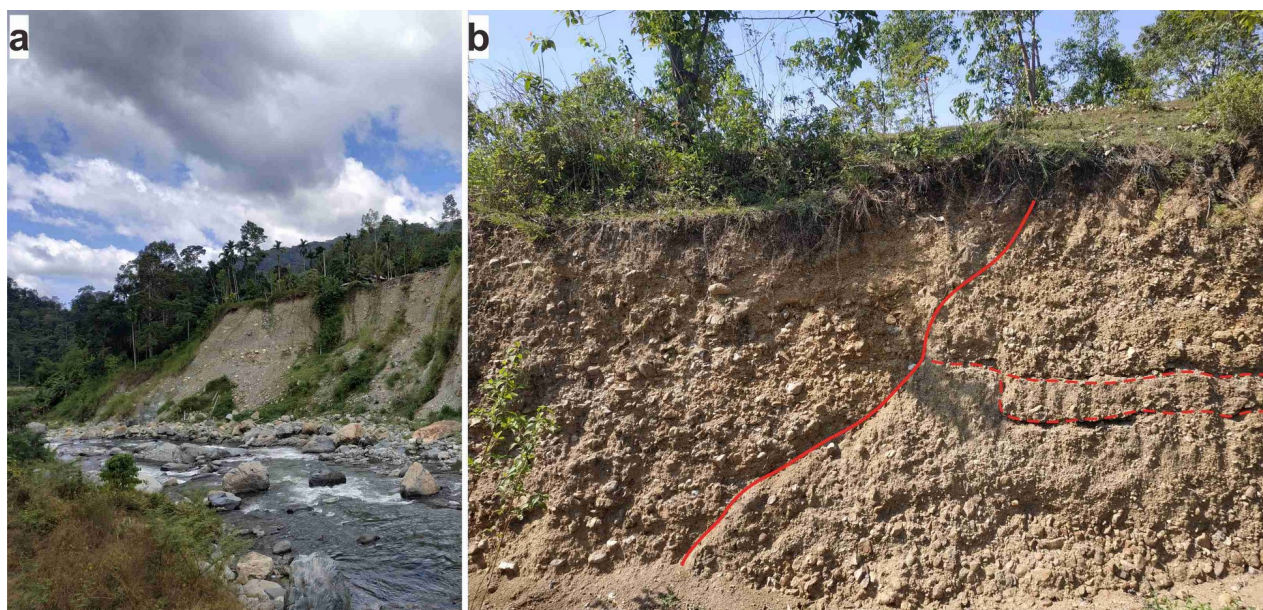


FIGURE 7. (a) Exposed alluvial terrace deposit in Tangse showing evidence of differential uplift across the fault. (b) Quaternary alluvial units disturbed by faults in Jantho, solid red lines indicate fractures, dashed red lines represent the boundary of sedimentary units.

4 km wide, according to several studies (Harris and Day, 1993; Wesnousky, 2006), would not stop a rupture on a fault, and thus cannot be considered as segment boundaries.

Continue to the northwest of Geumpang along the Aceh Fault segment is the Mane sub-segment. The total length of the fault is 18.8 km. At the beginning of the Mane sub-segment, the Aceh Fault meets the Seulimeum Fault segment. The junction area is characterized by higher seismicity (Umar *et al.*, 2018), indicating a relatively higher stress accumulation and release than other areas along the Aceh Fault zone. At km 113.6, the fault bend to to the right, forming a 0.35 km wide transpressional ridge. The Mane Fault is separated from the Jantho Fault on its northwest end by a 3.8 km wide left step-over.

The next segment, the Jantho Fault, is represented in the topography as a linear valley runs through the mountainous area between Tangse and Jantho villages (Figure 4b). This fault's total length is 33.6 km, with some minor 0.2–2 km wide right and left step-overs. At km 117, the fault movement is accommodated by several smaller faults forming a slightly wider fault zone. The Jantho sub-segment is terminated to the northwest, separated with Indrapuri sub-segments by a 5 km long fault discontinuation. The Indrapuri sub-segment is represented in

the topography as a slightly sinusoidal break of morphology (Figure 8a).

The northwesternmost section of the Aceh Fault is the Pulo Aceh sub-segment. The fault is recognized from the arrangements of the Pulo Aceh archipelago. The morphological lineaments of Aceh Fault segments on the offshore area is also observable through the bathymetry data, represented by a linear orientation of the bathymetric depth (Figure 8a).

5.2 Kinematic model of Aceh Fault segments

We interpret the Aceh Fault system's kinematics based on our field observations, by comparing previous studies' results, and analyzing their spatial geometric characteristic (Figure 5). Previous studies stated that the Aceh Fault has the same orientation as the GSF system ($\sim N 315^\circ E$) and is dominated by right-lateral strike-slip fault kinematics (Tabei *et al.*, 2015; Fernandez *et al.*, 2016). Our data indicate that the Aceh Fault system is dominated by a right-lateral strike-slip mechanism with a minor vertical slip. Some minor conjugate left-lateral faultings are also evident at some places. The right-lateral strike-slip faulting and orientation of the Aceh Fault segment are consistent with the expected orientation of horizontal displacement vectors as a result of the oblique convergence between Indo-Australian

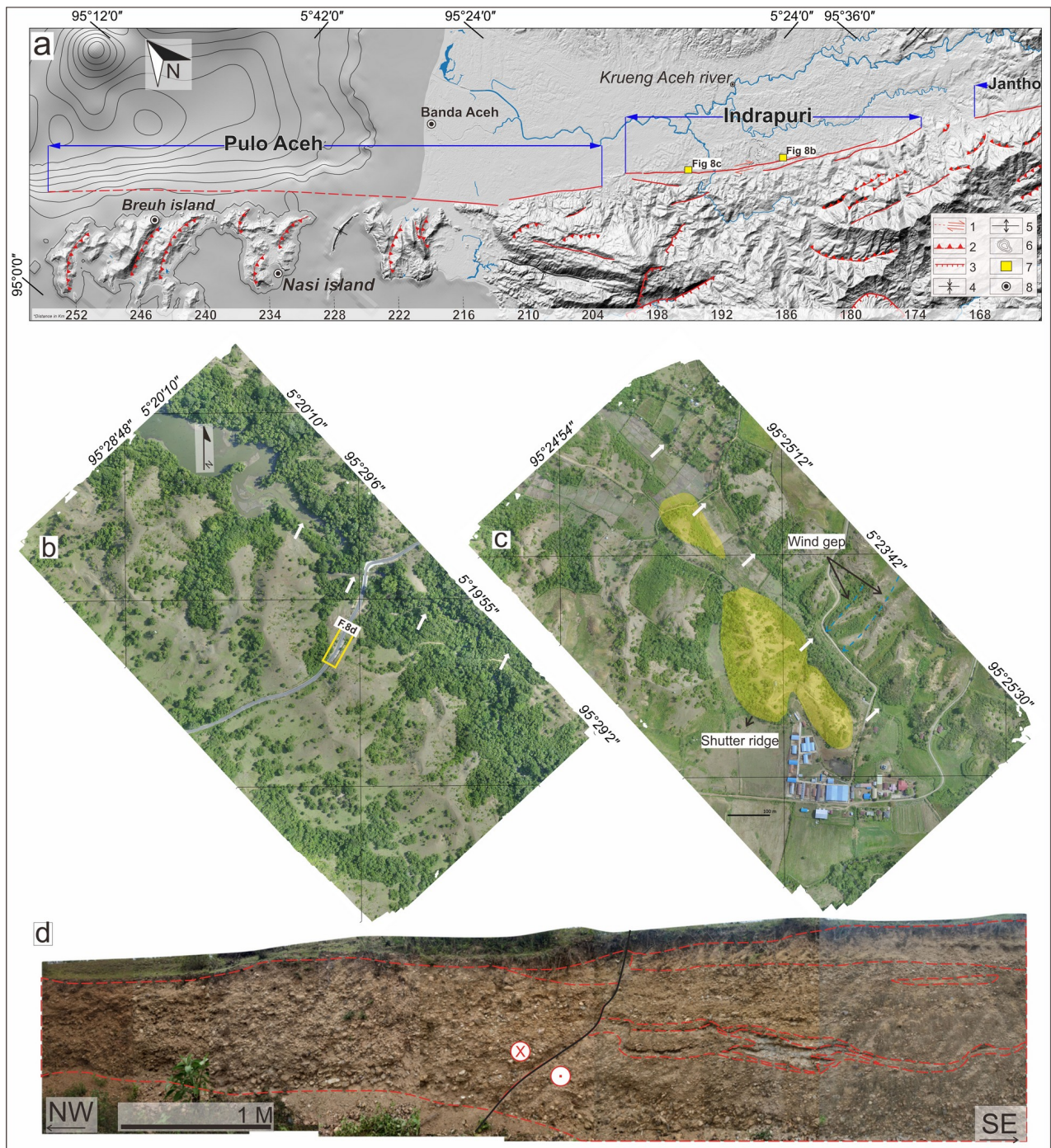


FIGURE 8. (a). Map of the Indrapuri and Pulo Aceh sub-segments. The notation of the inserted legend: (1) right strike-slip fault, (2) reverse fault, (3) normal fault, (4) syncline, (5) anticline, (6) Bathymetry contour, (7) Figures, (8) Area/city. (b) Aerial photography at Indrapuri sub-segment, yellow box indicate the location of Figure 7d. (c) the interpreted aerial photograph shows prominent morphology features. (d). Photomosaic of the fault trace exposed from a road excavation at the Indrapuri area, the red dashed line shows a layer of alluvium sediment. The black line represents the fault trace.

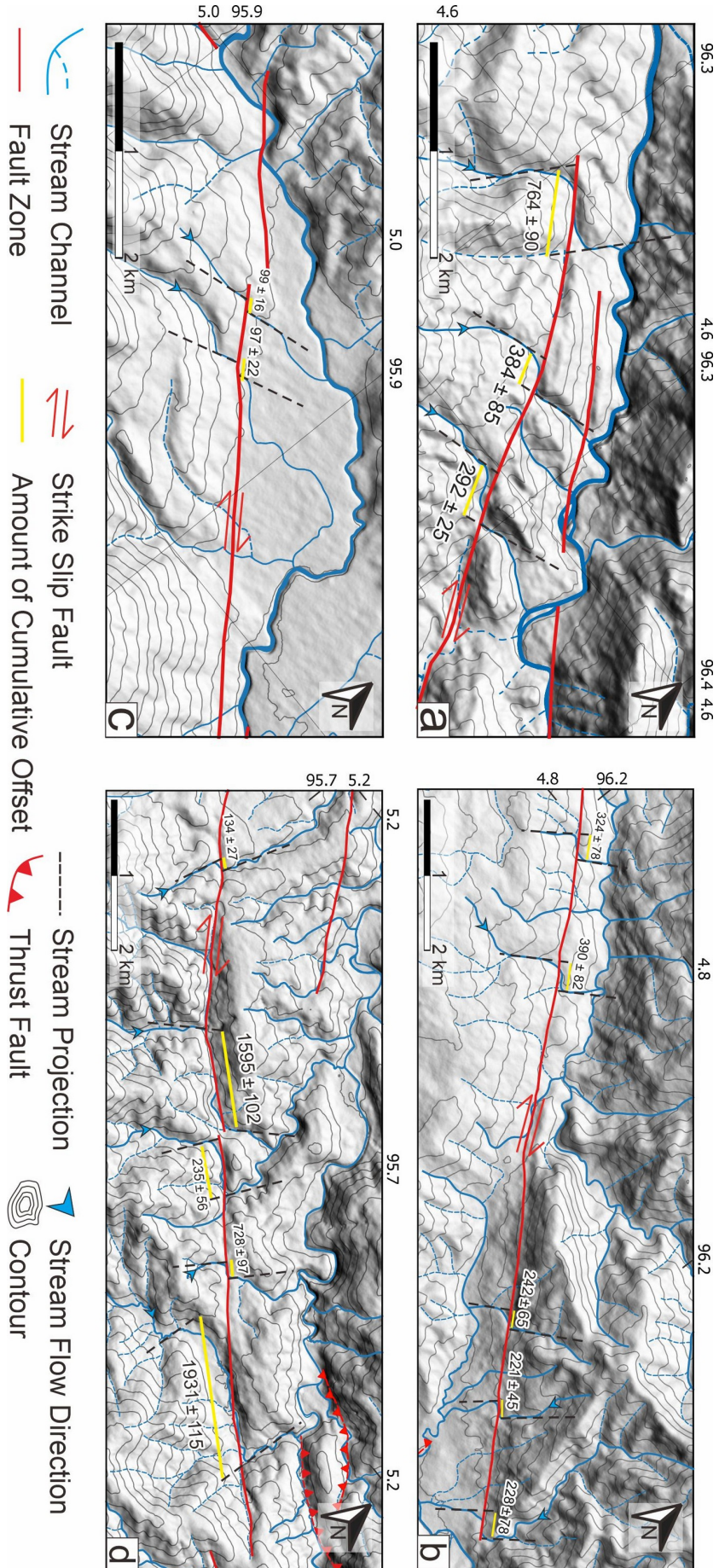


FIGURE 9. Hillshaded DEM showing area of our slip calculation. (a). Site 1 is located at the Kuala Tripa sub-segment. (b). Site 2 is located at Geumpang sub-segment. (c). Site 3 is located at Tangse sub-segment. (d). Site 4 is located at Jantho sub-segment.

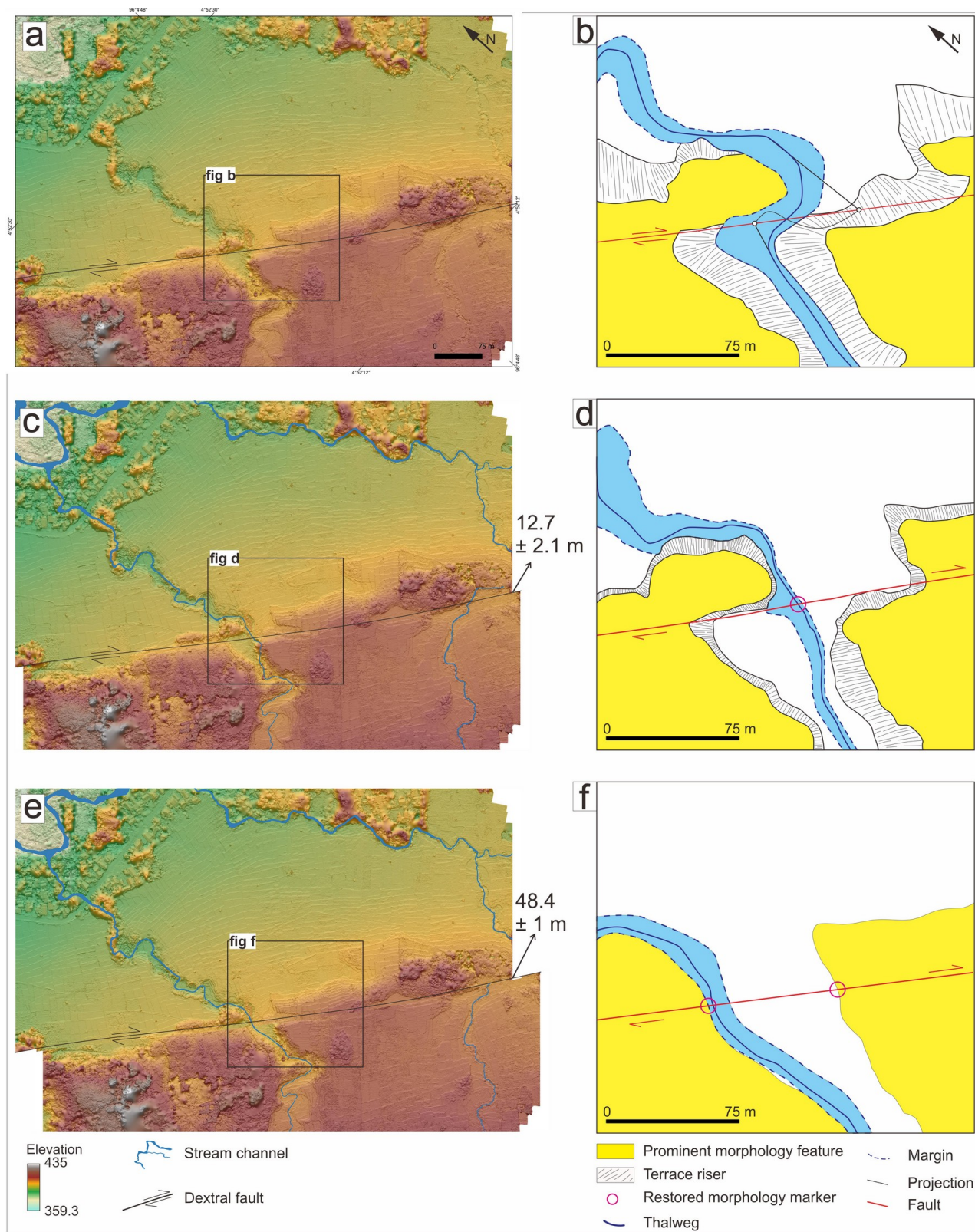


FIGURE 10. Successive back-slip reconstructions of a lateral offset channel at Geumpang sub-segment reconstructed using UAV-based DEM. We identified several geomorphic markers showing multiple amounts of displacement. (a) DTM of an area at km 89.5, where we observed a left lateral offset in a channel. (b) Interpreted geomorphology map showing the channel geometry relative to the fault strand as a base for uncertainty measurements. (c and d) Back calculation of separation of the youngest channel yield a 12.7 displacement. (e and f) Back calculation of separation based on hillslope morphology yielding a 48.4 m of displacement.

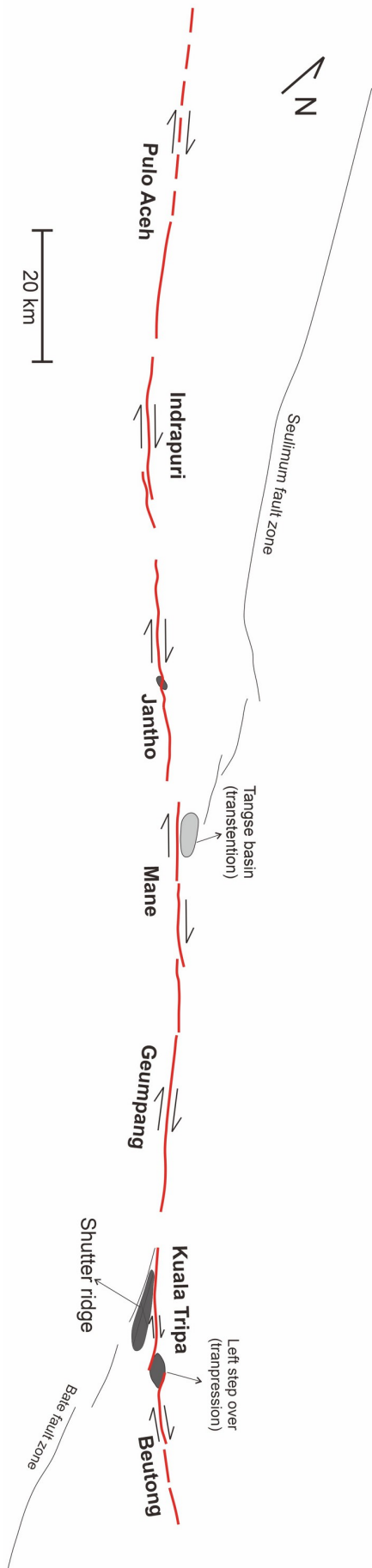


FIGURE 11. The updated segmentation model the Aceh Fault zone, where we divided the Aceh Fault into seven sub-segments. Dark grey represents a zone of uplift (transpression), and light gray show a zone of subsidence (translation) associated with fault bends and step-overs.

with Eurasia plates to the west of Sumatra island. Evidence of faulting on Quarternary age volcanic layers and sediments along the Aceh's sub-segments indicates that the fault is active (Figures 7b and 8d).

5.3 Estimation of maximum magnitude

We estimate the maximum magnitude of earthquakes based on an empirical formula developed by Stirling *et al.* (2008), which calculates seismic moments using the fault width and length. We adopt an 80° dip based on our field measurement. We assume a ~16 km depth seismogenic zone in this area, adopting the Umar *et al.* (2019) study.

The total length of the fault zone is ~250 km. Considering a depth of 16 km, and a dip of 80°, the rupture for the entire Aceh Fault would generate an M8.6 earthquake. This is unlikely given the geometrical arrangement of the fault. Our study suggests that the Aceh Fault is separated into seven smaller (15–50 km length) sub-segments that are likely to behave individually. The smallest estimated earthquakes along these fault segments are at M6.5 for the Kuala Tripa sub-segment. The estimated magnitude is slightly larger for Mane (M6.6), Beutong (M6.7), Indrapuri (M6.9), Jantho (M7.0), and Geumpang (M7.1) sub-segments. The largest estimated earthquake is at M7.2 along the Pulo Aceh Fault (Table 1).

The calculated cumulative offset along the Aceh Fault segments varies. The smallest identified offset is 12.7±2.1 m, measured at Geumpang sub-segment. The largest offset is measured at Jantho sub-segment, which shows a 1931±115 m horizontal offset. This may indicate an incomplete record or that the recorded offsets are a result of multiple earthquake events.

6 CONCLUSIONS

Based on the interpretation of the 8-m resolution DEM Nasional and BATNAS data, we suggest that the Aceh Fault segment is active and can be divided into seven sub-segments: (1) Beutong, (2) Kuala Tripa, (3) Geumpang, (4) Mane, (5) Jantho, (6) Indrapuri, and (7) Pulo Aceh. All of the fault sub-segments shows a dominant right-lateral strike-slip fault kinematics, with some minor oblique components.

TABLE 1. Summary of sub-segmentation and contributing magnitudes of the Aceh Fault.

Sub-segment	Segment boundaries	Length (km)	Width (km)	M_w^*
Beutong	left step-over, transpression ridge	19.0	16.24	6.7
Kuala Tripa	fault discontinuity	15.7	16.24	6.5
Geumpang	changes in fault orientation	38.3	16.24	7.1
Mane	left step-over	18.8	16.24	6.6
Jantho	fault discontinuity	33.6	16.24	7.0
Indrapuri	fault discontinuity	28.9	16.24	6.9
Pulo Aceh	fault discontinuity	50.0	16.24	7.2

* Estimation of moment magnitudes were calculated using equation (1) for slow slip movements of fault (Stirling *et al.*, 2008) where the width of the fault zone (W) is calculated using an assumption of 16 km of seismogenic depth and 80° of fault dip.

Each of the sub-segments is separated from each other either by steps, bends, or fault discontinuities. The sub-segments are varying in length from 15.7 to 50 km. We estimated, based on their fault length, that earthquake along these sub-segments will generate M6.5–7.2 earthquakes.

As observed in recent earthquakes along Sumatran Fault (Daryono *et al.*, 2012), a ~M6 along a fault will generate ~0.5 m of lateral displacement. Our calculation of cumulative lateral displacement of several channel offsets and shutter ridges yielding a range of 12.7±2.1 to 1931±115 m. Observing the amount of these offsets, it is likely that they are a result of multiple earthquakes, further investigation is necessary to decipher the amount of earthquakes recorded by these offsets.

Our high-resolution DEM from aerial photography allows us to map the fault in greater detail. Our updated segmentation model of the Aceh Fault segment provides new information regarding the geometry and a new estimation of the earthquake magnitude along the fault, which is important to improve the earthquake hazard analysis in the area. We identified several sites where lateral offsets are visible. This study provides a foundation for future slip-rate investigation along the Aceh Fault segment.

ACKNOWLEDGEMENTS

We thank the Department of Geological Engineering, Faculty of Engineering, Universitas Gadjah Mada, for providing funding for this study.

REFERENCES

- Bennet, J.D., Brige, D. McC., Cameron, N.R., Djunuddin, A., Ghazali, S.A., Jeffery, D.H., Kartawa, W., Keats, W., Rock, N.M.S., Thomson, S.J., and Whandoyo, R. 1981. Geological map of Banda Aceh sheet, scale 1: 250.000. Indonesian Geological Research and Development Center.
- Bemis, S.P., Micklethwaite, S., Turner, D., James, M.R., Akciz, S., Thiele, S.T., and Bangash, H.A. 2014. Ground-based and UAV-based photogrammetry: A multi-scale, high-resolution mapping tool for structural geology and paleoseismology. *Journal of Structural Geology*, 69, pp.163-178.
- Cameron, N.R., Bennett, J.D., Bridge, D.Mc.C., Clarke, M.C.G., Djunuddin, A., Ghazali, S.A., Harahap, H., Jeffery, D.H., Kartawa, W., Keats, W., Ngabito, H., Rocks, N.M.S., and Thompson, S.J. 1983. Geological map of Takengon sheet, Sumatra, scale 1: 250.000. Indonesian Geological Research and Development Center.
- Curry, J. R., 2005. Tectonics and history of Andaman Sea region. *J. Asian Earth Sci.*, 25, 187–232.
- Curry, J. R., Moore, D. G., Lawver, L. A., Emmel, F. J., Raitt, R. W., Henry, M., and Kieckhefer, R. 1979. Tectonics of Andaman Sea and Burma, in geological and geophysical investigations of continental margins. Edited by J. S. Watkins., L. Montadert., and P. W. Dickerson. Pp. 189–198, Amer. Assoc. Petrol. Geol. Memoir 29, Tulsa, Okla.
- Daryono, M. R., Natawidjaja, D., and Sieh, K. 2012. Twin-surface ruptures of the march 2007 M > 6 earthquake doublet on the Sumatran Fault. *Bulletin of the Seismological Society of America*, Vol. 102, No. 6, pp. 2356–2367.
- Duman, T. Y., Emre, O., 2013. The East Anatolian Fault: geometry, segmentation, and jog characteristics. *Geological Society*. London, Special Publications published online February 19, 2013, as DOI:10.1144/SP372.14.
- Fernández-Blanco, D., Philippon, M., and von

- Hagke, C., 2016. Structure and kinematics of the Sumatran Fault System in North Sumatra (Indonesia). *Tectonophysics* 693 (2016) 453–464.
- Harris, R. A., and Day, S. M., 1993. Dynamics of fault interaction—parallel strike-slip faults. *J. Geophys. Res.* 18, 4461–4472.
- Marliyani, G. I., Rockwell, T. K., Nathan, W., Onderdonk., and Sally, F., McGill, S. F. 2013. Straightening of the Northern San Jacinto Fault, California, as seen in the fault-structure evolution of the San Jacinto Valley step-over. *Bulletin of the Seismological Society of America*, Vol. 103, No. 3, pp. 2047–2061, June 2013, DOI: [10.1785/0120120232](https://doi.org/10.1785/0120120232).
- Marliyani, G. I., 2016. Neotectonics of Java, Indonesia: Crustal deformation in the overriding plate of an orthogonal subduction system. Doctoral dissertation, Arizona State University.
- Moechtar, H., Subiyanto., and Sufianto. 2009. Geologi alluvium dan karakter endapan pantai/pematang pantai di lembah Krueng Aceh, Aceh Besar. Pusat Survey Geologi.
- Sieh, K., and Natawidjaja, D., 2000. Neotectonics of the Sumatran fault, Indonesia. *Journal of Geophysical Research*, 105(B12): 28295. DOI: [10.1029/2000JB900120](https://doi.org/10.1029/2000JB900120).
- Singh, S. C., Moeremans, R., McArdle. J. and Johansen, K. 2013. Seismic images of the sliver strike-slip fault and back thrust in the Andaman-Nicobar region. *J. Geophys. Res. Solid Earth*, 118, 5208–5224, DOI: [10.1002/jgrb.50378](https://doi.org/10.1002/jgrb.50378).
- Stirling, M. W., Gerstenberger, M. C., Litchfield, N. J., McVerry, G. H., Smith, W. D., Pettinga, J., and Barnes, P. 2008. Seismic hazard of the Canterbury region, New Zealand: New earthquake source model and methodology. *Bull. N. Z. Soc. Earthquake Eng.*, 41, 51–67.
- Tabei, T., Kimata, K., Ito. T., Gunawan, E., Tsutsumi, H., Ohta, Y., Yamashina, T., Soeda, Y., Ismail, N., Nurdin, I., Sugiyanto, D., and Meilano, I. 2015. Geodetic and geomorphic evaluations of earthquake generation potential of the Northern Sumatran fault, Indonesia. *International Association of Geodesy Symposia*, DOI: [10.1007/1345_2015_200](https://doi.org/10.1007/1345_2015_200).
- Umar, M., Bauer, K., Muzli, M., Ryberg, T., Nurdina, I., Masturiyono, M., and Weber, M. 2019. Aceh-Seis project provides insights into the detailed seismicity distribution and relation to fault structures in Central Aceh, Northern Sumatra. *Journal of Asian Earth Sciences*. 171 (2019) 20–27.
- Umar, M., Irwandi., Rusydy, I., Muzli., Erbas, K., Marwan., Asrillah., Muzakir., and Ismail, N. 2018. Investigation of Aceh Segment and Seulimeum Fault by using seismological data; A preliminary result. *The International Conference on Theoretical and Applied Physics*, DOI: [10.1088/1742-6596/1011/1/012031](https://doi.org/10.1088/1742-6596/1011/1/012031).
- Wesnousky, S. G., 2006. Predicting the endpoints of earthquake ruptures. *Nature*, 444 (7117): 358–360. DOI: [10.1038/nature05275](https://doi.org/10.1038/nature05275).